We are IntechOpen, the world's leading publisher of Open Access books
Built by scientists, for scientists

6,900
Open access books available

185,000
International authors and editors

200M
Downloads

154
Countries delivered to

Our authors are among the

TOP 1%
most cited scientists

12.2%
Contributors from top 500 universities

CLARIVATE ANALYTICS
BOOK CITATION INDEX
INDEXED

WEB OF SCIENCE™

Selection of our books indexed in the Book Citation Index
in Web of Science™ Core Collection (BKCI)

Interested in publishing with us?
Contact book.department@intechopen.com

A Respiratory Motion Prediction Based on Time-Variant Seasonal Autoregressive Model for Real-Time Image-Guided Radiotherapy

Kei Ichiji, Noriyasu Homma, Masao Sakai, Makoto Abe, Norihiro Sugita and Makoto Yoshizawa

Additional information is available at the end of the chapter

http://dx.doi.org/10.5772/56554

1. Introduction

In radiation therapy, to deliver continuously a sufficient radiation dose to target volume yields a better therapeutic effect. While, avoiding an exposure to healthy tissues surrounding the target volume is also an important requirement for suppressing the adverse effect. Image-guided radiation therapy (IGRT) has potential to achieve the two requirements and as it's application, stereotactic body radiation therapy (SBRT) has been used in clinic. In SBRT, the irradiated field is positioned with millimeter accuracy by proper daily setup. The accurate irradiation can allow the increase of radiation dose by ignoring the irradiation to the healthy tissues. Indeed, it has been reported that the treatment result of SBRT is comparable to the outcome from surgery [1].

As mentioned above, the higher accuracy as irradiation allows the higher planning dose to the target. However, intra-fractional organ motion, such as respiratory motion of lung, often makes misalignment of the isocenter and the target volume during treatment fraction. For example, respiratory motion moves lung tumor over 10 mm per second [2, 3]. In this case, the irradiation error caused by intra-fractional motion is not negligible in terms of adverse effect. Therefore, the respiratory motion management is a very important task in the field of radiation treatment [4].

To take into account the intra-fraction motion of lung tumor, some irradiation techniques have been investigated. The technique most widely used is the use of internal target volume (ITV) [5]. ITV includes internal margin determined by the intra-fractional organ motion. Consequently ITV covers the target volume CTV without misalignment as shown in Figure 1). However, radiation dose must be lower than the case of the irradiation without internal margin, because the irradiated area also covers normal tissues surrounding the target volume. On the other hand, a gating technique can give a high radiation dose to the lung tumor [6, 7].
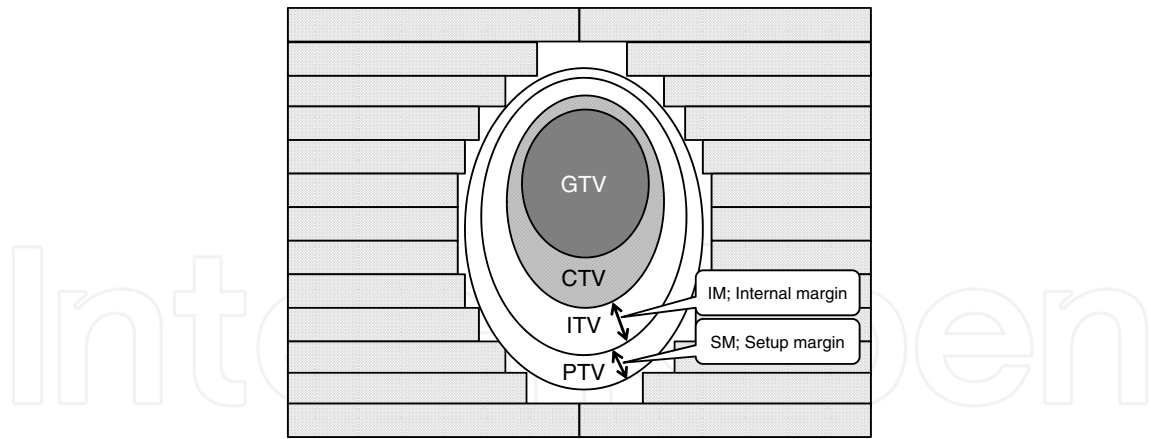
Figure 1. A relationship between target volumes. GTV; gross tumor volume. CTV; clinical tumor volume. ITV; internal target volume. PTV; planning target volume.
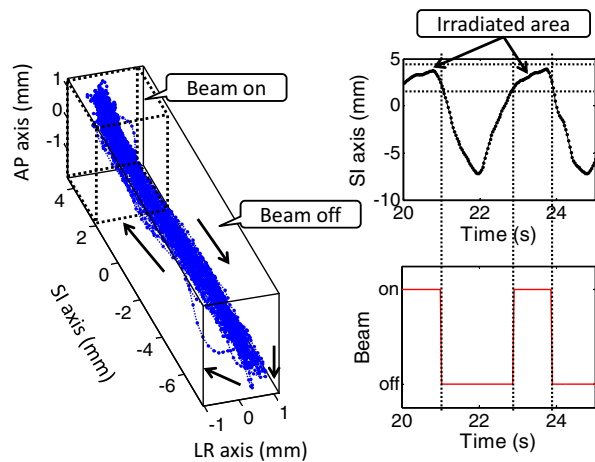

Figure 2. A schematic diagram of gated radiotherapy. The dots denotes a three-dimensional tumor trajectory. Irradiation is interrupted when the tumor is out of the region drawn as dotted line. AP, SI, and LR denotes anterior-posterior, superior-inferior, and left-right axes, respectively.

This is on-and-off irradiation to static region as shown in Figure 2. The radiation dose is delivered when the target volume is within the area planned preliminarily, and the irradiation interrupts if the target volume is out of the planned area. The gating technique can suppress the exposure to healthy tissues and allows high-dose-rate irradiation which is sufficient to yield a better therapeutic effect. However, instead of high-dose exposure, the gating takes longer treatment time to yields same therapeutic effect to SBRT due to the interruption.

An ideal irradiation to the moving target is to continuously irradiate a sufficient dose to the tumor which can be achieved by controlling the radiation beam to chase the moving target [8]. Such real-time tumor following (or chasing) irradiation yields an ideal therapeutic effect and can shorten the treatment duration. A schematic diagram of the tumor following irradiation is shown in Figure 3.

The tumor following irradiation requires the following two key techniques at least.

(i) Real-time measurement of tumor position and shape.

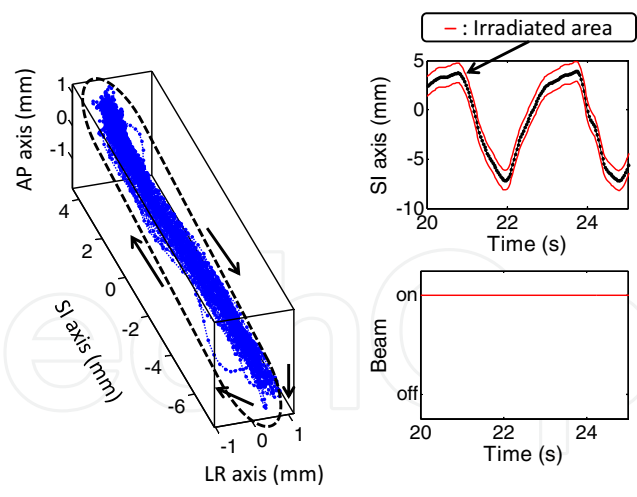(ii) Real-time repositioning and reshaping the treatment beam

Figure 3. A schematic diagram of tumor following radiotherapy. The dots denotes a three-dimensional tumor trajectory. Moving tumor is continuously irradiated as the region drawn as dotted line. AP, SI, and LR denotes anterior-posterior, superior-inferior, and left-right axes, respectively.
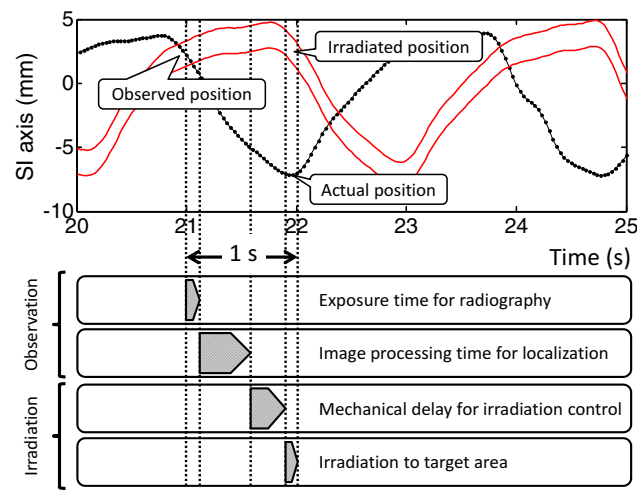

Figure 4. A schematic diagram of the tumor following irradiation with system latency. In this example, the total delay is 1 s and the delay distances the target tumor from the irradiated area over 10 mm.

The first technique for tumor localization has been achieved by using an X-ray fluoroscopic imaging system such as real-time tumor tracking system [7]. The second technique of beam-positioning systems can be realized by using dynamic multi-leaf collimator, robotic couch, robotic manipulator, and so on. However, the tumor following irradiation has not been developed clinically yet. This is because even we can obtain the precise lung tumor position in real-time, current radiotherapy machine has mechanical and computational time delays of up to about 1 s for controlling the irradiation field and image processing [9]. The latency can definitely affect badly on the irradiation accuracy [10], and must be compensated. Figure 4 shows a schematic diagram of the tumor following irradiation without delay compensation.

Prediction of future lung tumor motion is a typical solution for compensating the system latency and thus is a hot research topic for the tumor following irradiation. Then, the third technique is needed to develop the tumor following radiation therapy.

(iii) Real-time motion prediction

Several prediction methods have thus been proposed for the respiratory motion. These include linear regression [11, 12], extrapolation [11], artificial neural network [11, 13], Kalman filter [11], nonlinear regression based on the Takens theorem [12, 14], probabilistic modeling [15, 16] and so on. More details can be found in a literature such as a survey study of the prediction of lung tumor motion [17]. A variety of the prediction approaches indicates that there is currently no best prediction method in clinical use because of the insufficient accuracy.

In general, the prediction is realized as an application of time series analysis. General prediction methods, such as autoregressive moving average (ARMA) model [18], require a stationarity of the target time series. However, the respiratory motion essentially has complex and time-varying characteristics. For example, the repetition of inhalation and exhalation naturally involves periodicity, but the periods are time-varying. Nevertheless the periodic component can still help to predict the motion because the past observed motion will arise again at periodic intervals. It means that we can predict the motion accurately if the period of target motion is obtained. Thus, the use of the periodicity can be a good approach to predict the respiratory motion.

The methods that focus on periodic components in respiratory motion have been developed as seasonal autoregressive (SAR) model-based method [19] and periodic ARMA model-method [20]. However, the periodicity in the respiratory motion fluctuates with time, and the adaptation of these methods to time-variant periodic variation seems insufficient yet. For example, SAR model-based method converts the target motion with time-variant period to a new motion with constant period to use the SAR model properly. But if the conversion from time-variant to constant period is incomplete, the prediction accuracy can decrease. On the other hand, the periodic ARMA estimates the period of the target motion by using long historical samples of 60 s. However, the use of long historical samples causes a hysteresis and cannot trace the change of the periodicity. Therefore, to adapt to the time-varying periodicity still remains as a challenge to accurately predict the respiratory motion.

In this chapter, to predict the respiratory motion by use of its periodicity, a time-variant seasonal autoregressive (TVSAR) model-based method is proposed [21]. The proposed method can model the time-variant periodicity more precisely, and we adopt only a small number of samples to suppress the hysteresis. In the next section, we briefly describe the characteristics of the lung tumor motion. Then, in section 3, TVSAR model is explained. The model is based on SAR, but is newly developed to adapt to the fluctuated periodicity by using unequally-spaced intervals instead of multiples of the constant period. To show the prediction performance of TVSAR model-based method, experimental result by using some clinical data sets of lung tumor motion is described in section 4. Section 5 provides concluding remarks.

2. Respiratory motion of lung tumor

Figure 5 shows an example of time series of respiratory motion of lung tumor. The time series of tumor motion was observed as a location of the golden fiducial marker implanted into around the tumor, by using a kV X-ray fluoroscopic imaging system known as RTRT system, with sampling frequency 30 Hz, at Hokkaido University Hospital, Sapporo, Japan [7].

In general, a lung tumor motion involves a periodical component because breathing is composed of repetition of inspiration and expiration. Figure 6 provides power spectrum density (PSD) of the tumor motion shown in the top of Figure 5. The dominant frequency
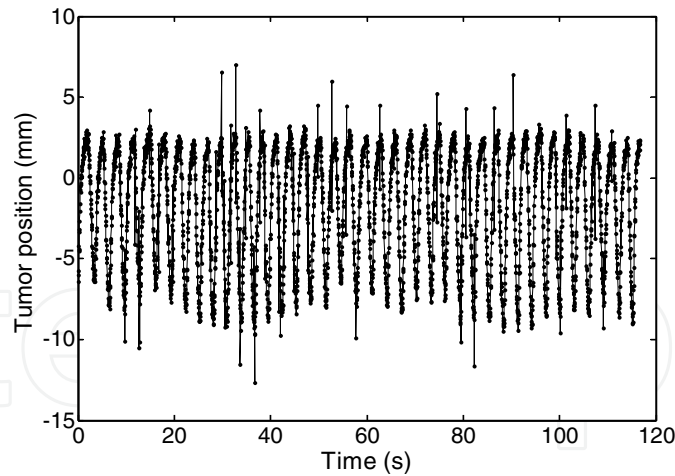
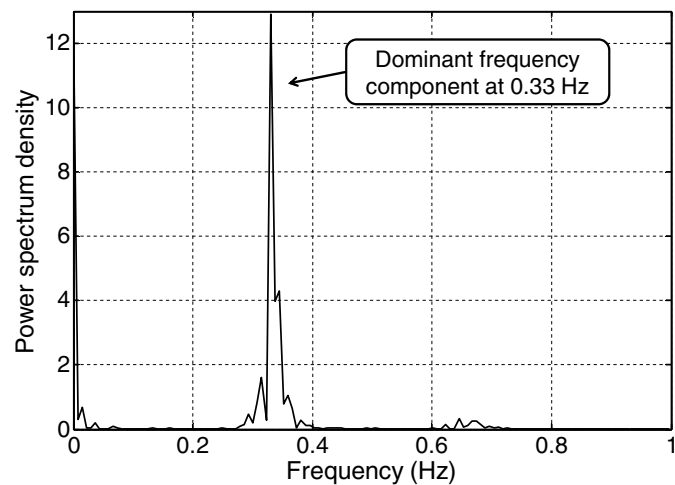**Figure 5.** An example of time series of lung tumor motion.

Figure 6. Power spectrum density of the respiratory induced tumor motion shown in Figure 5. The dominant frequency component is found at 0.33 Hz.

corresponding to the respiratory cycle can be found at 0.33 Hz approximately in this example. This means that the tumor motion has a periodical component induced by the 3 s respiratory cycle in average.

As is clear from the analysis, one of dominant components in respiratory motion is periodic variation due to repetition of inhalation and exhalation. However, the period of the motion is not constant, but a time varying function. Such quasi-periodical nature of the motion is simply found as fluctuation of peak-to-peak intervals. For example, time interval between a peak and next peak differs each other even if the amplitude variation is sufficiently small as shown in Figure 7. This suggests that the dominant frequency is time-varying.

Recalling that the breathing period is time-variant, short-time Fourier transform (STFT), instead of the normal long-time Fourier transform, was performed on the motion example. The time-variation of the frequency spectrum is shown in Figure 8. The dominant frequency at each time is depicted as black dashed line. The line clearly indicates that the respiratory cycle fluctuates with time. The range of the fluctuation was from 0.298 to 0.360 Hz in this example.
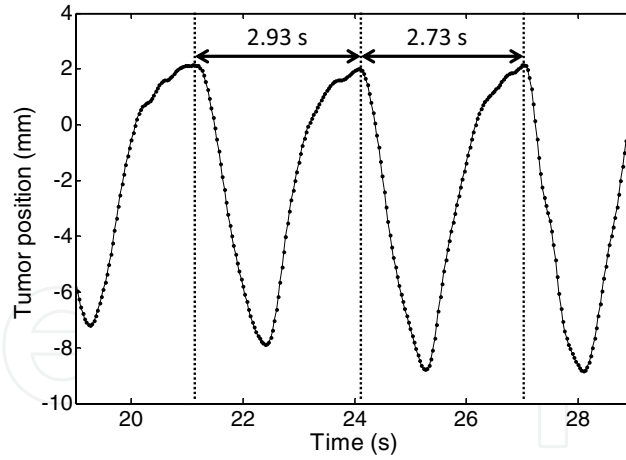
Figure 7. An example of fluctuated periodicity of respiratory motion. The peak to peak intervals indicated as double-headed arrows are not same to each other.
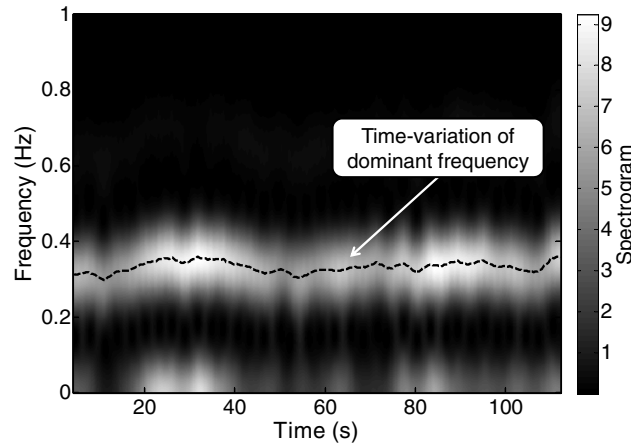

Figure 8. Time-variation of power spectrum density. The dominant frequency fluctuates with time. The range of fluctuation is from 0.298 to 0.360 Hz in this example.

3. Prediction methods

The periodicity found in the respiratory motion is a typical one of nonlinear and complex nature but also it can be useful to predict itself. That is, the past observed patterns in the motion will repeatedly arise at constant period. In this section, seasonal autoregressive (SAR) model is explained as a method with use of periodicity. Also, a limitation of general SAR model for lung tumor motion prediction is shown. Then, time-variant SAR model is introduced as a method designed for tumor motion prediction.

3.1. Seasonal autoregressive (SAR) model

Seasonal autoregressive integrated moving-average (SARIMA) model [22] is a general expression of the time series which changes periodically (i.e., a periodical function of time such that $x(t) \sim x(t - \rho \cdot s)$).

The SARIMA model of the time series $\{x(0), x(1), \ldots, x(T)\}$ with period s sample can be expressed as follows.

$$\phi(B)\Phi(B^s)(1 - B)^d(1 - B^s)^D x(t) = \theta(B)\Theta(B^s)\epsilon(t) \tag{1}$$

where d and D are respectively the order of local and seasonal integrated components, $\epsilon(t)$ is the Gaussian noise of which mean and variance are 0 and σ^2, respectively, and B is a delay operator defined by

$$B^k x(t) = x(t-k), \ k = 1, 2, \ldots \tag{2}$$

Then, each components of the SARIMA model are given as follows.

$$\text{Autoregressive: } \phi(z) = 1 - \phi_1 z - \cdots - \phi_p z^p \tag{3}$$
$$\text{Moving-average: } \theta(z) = 1 + \theta_1 z + \cdots + \theta_q z^q \tag{4}$$
$$\text{Seasonal AR: } \Phi(z) = 1 - \Phi_1 z - \cdots - \Phi_P z^P \tag{5}$$
$$\text{Seasonal MA: } \Theta(z) = 1 - \Theta_1 z + \cdots + \Theta_Q z^Q \tag{6}$$

where p, q, P and Q are the orders of four components in (3)-(6) respectively.

The SARIMA model can express various periodical time series by designing the model parameters. In the followings, let us consider only the seasonal autoregressive (SAR) component to avoid the over fitting problem and to simplify the explanation of the prediction method. That is, let $p = q = Q = d = D = 0$ in (1), then for this special case, we can obtain SAR model for the time series $y(t)$ as follows.

$$y(t) = \epsilon(t) + \sum_{\rho=1}^{P} \Phi_\rho \cdot y(t - \rho \times s) \tag{7}$$

where P is the order of the SAR components, $\Phi_\rho, \rho = 1, 2, \ldots, P$ are the SAR coefficients, and s are the constant period of the target time series.

Then, to substitute $t + h$ for t, the prediction equation by using (7) can be given by

$$\hat{y}(t + h | t) = \sum_{\rho=1}^{P} \Phi_\rho \cdot y(t + h - \rho \times s) \tag{8}$$

where $\hat{y}(t + h | t)$ is the predicted value of future time $t + h$ samples with h samples ahead of current time t, and the term $-\rho \times s + h$ must be not longer than 0 for composing the prediction by using only past observations.

The equations (7) and (8) show that an essential core of the general SAR depends on an assumption that each values of the same phase correlate each other. These equations can provide a simple description with a single model for the periodical variation with period s. For example, if target time series are given by the following deterministic and fully periodical function:

$$x(t) = A_0 + \sum_{n=1}^{N} A_n \cdot \cos\left(2\pi \frac{n}{s} t - \varphi_n\right) \tag{9}$$

where $A_n, n = 0, 1, 2, \ldots$ and $\varphi_n, n = 1, 2, 3, \ldots$ are amplitudes and initial phases for each n-th harmonic component, respectively. Then, let $\Phi_\rho = 1/P$ in Eq. (8), the SAR model can well
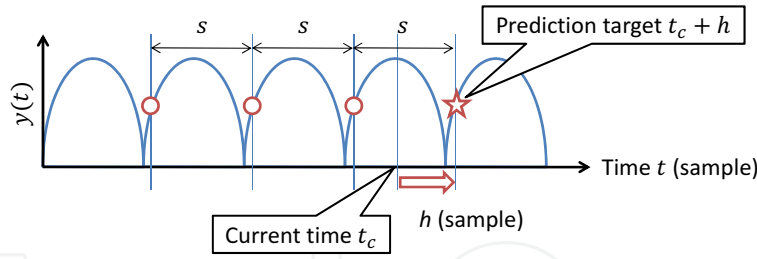
Figure 9. Schematic diagram of SAR model-based prediction for time series with constant period.
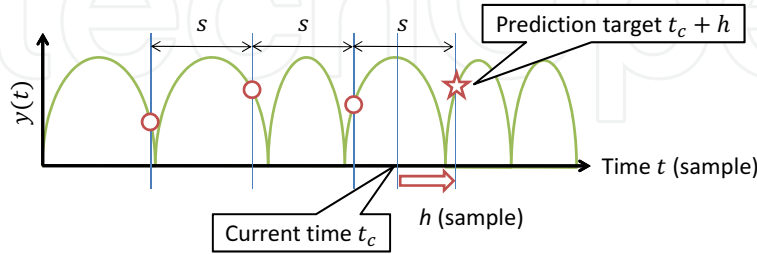

Figure 10. Schematic diagram of SAR model-based prediction for time series with fluctuated period.

predict the future value of the periodical function $x(t+h)$ at h-sample ahead future as follows.

$$
\begin{aligned}
\hat{x}&(t+h|t) \\
&= \frac{1}{P} \sum_{\rho=1}^{P} \left(A_0 + \sum_{n=1}^{N} A_n \cdot \cos \left(2\pi \frac{n}{s}(t+h-\rho \cdot s) - \varphi_n \right) \right) \\
&= \frac{1}{P} \sum_{\rho=1}^{P} \left(A_0 + \sum_{n=1}^{N} A_n \cdot \cos \left(2\pi \frac{n}{s}(t+h) - 2\pi\rho - \varphi_n \right) \right) \\
&= \frac{1}{P} \sum_{\rho=1}^{P} \left(A_0 + \sum_{n=1}^{N} A_n \cdot \cos \left(2\pi \frac{n}{s}(t+h) - \varphi_n \right) \right).
\end{aligned}
\tag{10}
$$

Figure 9 shows a schematic diagram of SAR model-based prediction for simple periodic time series with period s. In this example, SAR model can predict the target value (drawn as star) by referring the past observed values (drawn as circles) which are similar to the target value by using constant period s.

As shown by the prediction example, the SAR model-based equation (8) is useful and powerful to predict unknown future value of periodic time series. Then, remember that the dominant component in respiratory tumor motion is periodical component. These facts suggest that the SAR model is suitable to predict the tumor motion. However, remember that the periodicity in our target time series, lung tumor motion, fluctuates. The use of constant period s in equation (8) may be improper for the tumor motion. That is, if the periodical nature in the target time series changes with time, the constant period will provide a large prediction error.

A simple solution for adapting the SAR model to the fluctuated periodicity is to substitute a time-variant period $s(t)$ for the constant period s given by

$$
\hat{y}(t) = \epsilon(t) + \sum_{\rho=1}^{P} \Phi_\rho \cdot y(t - \rho \cdot s(t)).
\tag{11}
$$

Then the new prediction equation is written as

$$\hat{y}(t+h|t) = \sum_{\rho=1}^{P} \Phi_\rho \cdot y(t+h-\rho \cdot s(t+h)). \tag{12}$$

The equation above is about the same to the SAR model-based method [19] and it seems that it can adapt to the fluctuated periodicity, but this simple extension of SAR model has a limitation.

For explanation of the limitation, let us consider time series with a time-varying period as a function of time t. For this situation, the instantaneous phase $\vartheta(t)$ of the time series is given as a time-integration of the angular velocity $\omega(t)$, such as $\vartheta(t) = \int_0^t \omega(t)dt$. If the angular velocity is given as a linear function of time t,

$$\omega(t) = \omega_a t + \omega_0, \tag{13}$$

where ω_a and ω_0 are constants. And the instantaneous phase is given a nonlinear (the second-order in this case) function as

$$\vartheta(t) = \frac{1}{2}\omega_a t^2 + \omega_0 t. \tag{14}$$

Then let us assume that $s(t)$ is known or estimated correctly. That is, the term $s(t)$ can refer the instantaneous phase same to the target time t, i.e., $\vartheta(t) = \vartheta(t-s(t))$ However, the terms $\rho \cdot s(t), \rho = 2, 3, \ldots, P$ in (11) cannot refer the same instantaneous phase, i.e., $\vartheta(t) \neq \vartheta(t - \rho \cdot s(t)) + 2\pi\rho$, even if the $s(t)$ is given as a true value.

Thus, the simple SAR model-based solution by using the time-varying period $s(t)$ cannot express the fluctuated periodic nature suitably, even if the change of the periodicity is sufficiently simple such as a linear function of time. This is one of the limitations of SAR model in the prediction of fluctuated periodical time series such as respiratory tumor motion.

3.2. Time-variant SAR (TVSAR) model

To overcome the limitation of the general SAR model, a time-variant SAR (TVSAR) model for prediction of the lung tumor motion has been proposed [21]. The TVSAR equation corresponding to (7) can be expressed as

$$y(t) = \epsilon(t) + \sum_{\rho=1}^{P} \Phi_\rho \cdot y(t-r_\rho(t)). \tag{15}$$

where $r_\rho(t)$ are reference intervals of the ρth order at time t.

The reference intervals $r_\rho(t)$ can be defined as a time interval between the current time and the corresponding past time which has the same phase to the current one. In other words, if an instantaneous phase $\vartheta(t)$ of the time series is given, the reference intervals can be defined as follows.

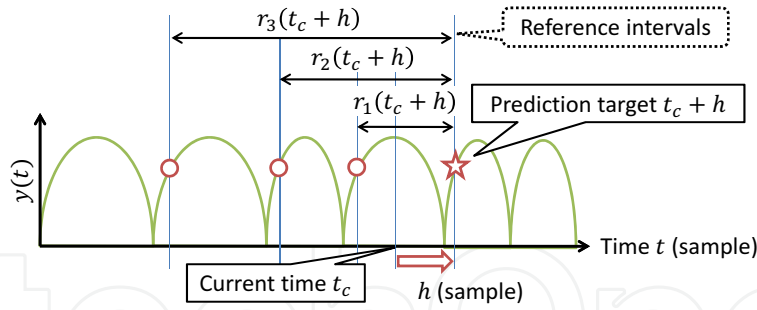$$r_\rho(t) = \arg\min_{k>0} |\vartheta(t) - 2\rho\pi - \vartheta(t-k)| \tag{16}$$

Figure 11. Schematic diagram of time-variant SAR (TVSASR) model-based prediction for time series with fluctuated period.
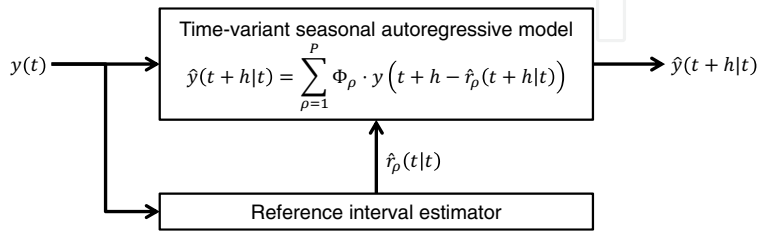

Figure 12. Schematic diagram of TVSAR model-based prediction system.

Also, if the period is a constant, the reference interval can be expressed by

$$r_\rho(t) = \rho \times s, \text{ if } \frac{d\vartheta(t)}{dt} = \frac{2\pi}{s}. \tag{17}$$

Note that, the constant reference interval shown by (17) corresponds to that used in the general SARIMA equations of (7) and (8).

Then, an ideal prediction equation of the time-variant SAR is expressed by substituting $t + h$ for t as follows.

$$\hat{y}(t + h|t) = \sum_{\rho=1}^{P} \Phi_\rho \cdot y(t + h - r_\rho(t + h)) \tag{18}$$

where the term $h - r_\rho(t + h) \leq 0$.

Figure 11 shows a schematic diagram of TVSAR model-based prediction. The reference intervals can refer the past values observed which are corresponding to the target value, on the time series with fluctuated period. Also, Figure 12 shows TVSAR model-based prediction system.

Note that, in (18), we have to know the reference interval at h sample ahead future, but it is unknown in practice. In this case, we need to estimate it. The estimation method will be explained in the next section.

3.2.1. Online estimation of reference intervals: Short-time correlation analysis

In TVSAR model, the reference interval $r_\rho(t)$ is an important factor to predict the lung tumor motion accurately, and must be estimated on-line. In this study, a correlation analysis is adopted to estimate the reference interval.

The correlation analysis based estimation procedure of the reference interval is as follows.

1. Calculate a correlation function between the latest subset

$$\{y(t-w), y(t-w+1), \ldots, y(t-1), y(t)\} \tag{19}$$

and k-sample lagged subset

$$\{y(t-k-w), y(t-k-w+1), \ldots, y(t-k-1), y(t-k)\} \tag{20}$$

where w is a window length for subset time series. The correlation function is given by

$$\gamma(t,k) = \frac{1}{w} \sum_{j=0}^{w-1} \frac{y(t-j) - \mu_t}{\sigma_t} \frac{y(t-k-j) - \mu_{t-k}}{\sigma_{t-k}} \tag{21}$$

Here μ_t and σ_t are the sample mean and standard deviation of the subset time series.

2. The estimated reference intervals $\hat{r}_\rho(t|t)$ can be obtained by the intervals between $k = 0$ and the peak points of the correlation function $\gamma(t,k)$ corresponded to each seasonal order ρ:

$$\hat{r}_\rho(t) = \arg \max_{r_\rho(t-1)-l \leq k \leq r_\rho(t-1)+l} \gamma(t,k) \tag{22}$$

where l defines the search area for the peak of $\gamma(t,k)$.

3. The window length is updated at each time by using the latest estimation of the first order reference interval as

$$w = \text{round}(0.5\hat{r}_1(t|t)). \tag{23}$$

Note that the windows length can affect the accuracy and response time to estimate the fluctuated periodicity. In this study, the window length was empirically set as almost half of single wave.

The initial condition is defined as follows.

$$\hat{r}_\rho(1|1) = \rho \times \bar{s}, \tag{24}$$

$$w = \text{round}(0.5\hat{r}_1(1|1)) \tag{25}$$

where $\bar{s}$ is the average of pre-observed time variant periods of the time series. $\bar{s} = 90$ sample was used for this study.

An example of the correlation function and estimated reference intervals are shown in Figure 13. The reference intervals are thus estimated as intervals from lag 0 to ρ-th local maximum points of the correlation function.

Time-variation of the correlation function and estimated reference intervals are shown in Figure 14. As is clear from this figure, reference intervals of lung tumor motion intricately change with time evolution.

We can now estimate the reference intervals, but we need future value of them for (18). According to the figure 14, these reference intervals also fluctuate intricately and those prediction is difficult. So $r_\rho(t+h)$ cannot be directly used for the prediction in (18). As a realistic way, we simply extrapolated $r_\rho(t+h)$ from the current estimation $\hat{r}_\rho(t|t)$ with zero-order hold: $\hat{r}_\rho(t+h|t) = \hat{r}_\rho(t|t)$. Then, (18) can be rewritten as

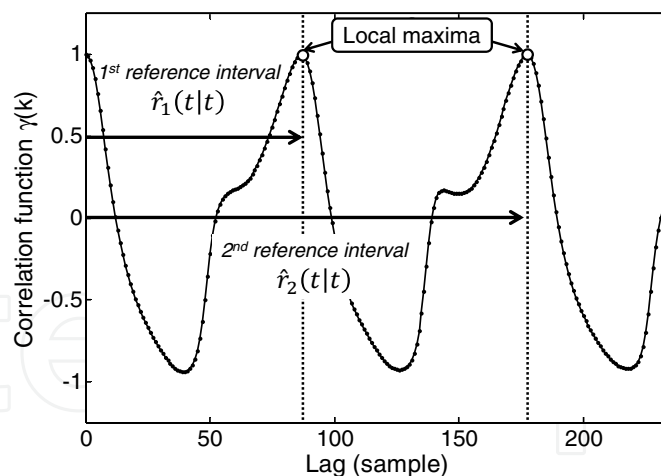$$\hat{y}(t+h|t) = \sum_{\rho=1}^{P} \Phi_\rho \cdot y(t+h-\hat{r}_\rho(t|t)). \tag{26}$$

Figure 13. An example of the correlation function $\gamma(t,k)$ and estimeted reference intervals $r_\rho(t), \rho = 1$ and 2 for the tumor motion shown in Figure 5.
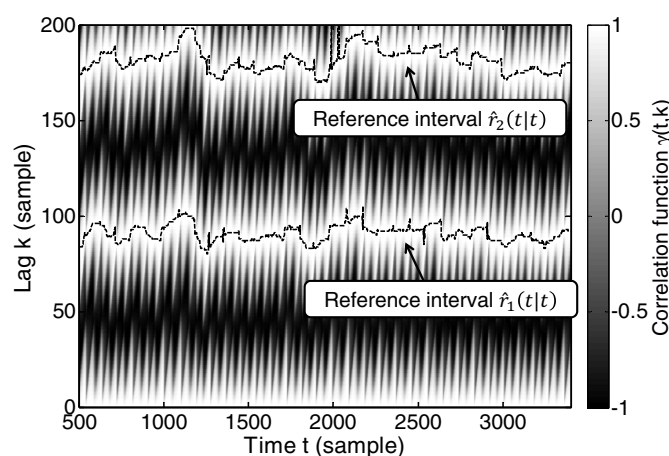

Figure 14. Time-variation of the correlation function $\gamma(t,k)$ and estimated reference intervals $r_\rho(t), \rho = 1$ and 2 for the tumor motion shown in Figure 5.

4. Experimental results

To evaluate the prediction performance of the methods described in Section 3, a prediction experiment by using clinical data sets was performed.

4.1. Experimental setup

4.1.1. Clinical data sets of lung tumor motion

Three data sets of respiratory tumor motion time series were used for the experiment. All the data sets were observed with sampling frequency $F_s = 30$ Hz and provided by Hokkaido University Hospital. Note that, a part of the data sets and measuring condition have been already shown in Section 2. Each data sets include three time series that correspond to spatial axes; left-right (LR), superior-inferior (SI), and anterior-posterior (AP) axes, respectively. The observational noises included in original data sets were preliminarily eliminated by using the statistical and low-pass filters. Figure 15 shows the three data sets and Table 1 summarizes data sets characteristics.
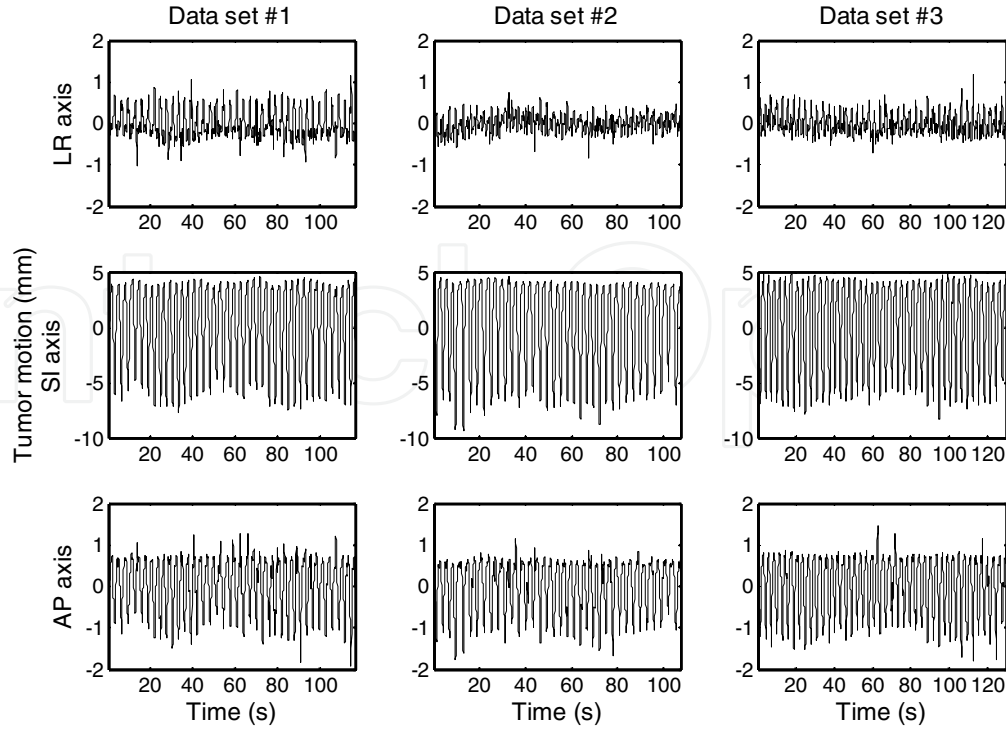
Figure 15. Three data sets of lung tumor motion. Each rows correspond to LR: left-right, SI:
superior-inferior, and AP: antero-posterior axes.

4.1.2. Tested methods

For comparison of the prediction performance, the following four methods were tested.

1. Zero-order hold (ZOH) method assumes that the latest position of tumor will not change
   in future. The prediction equation is given by

$$\hat{y}(t + h|t) = y(t). \tag{27}$$

   Note that the use of ZOH corresponds to the case that the system latency in radiotherapy
   machine is not compensated.

2. First-order hold (FOH) method assumes that the latest position and velocity will not
   change in future. The prediction equation is given by

$$\hat{y}(t + h|t) = y(t) + (y(t) - y(t - 1)) h. \tag{28}$$

3. Seasonal autoregressive (SAR) model-based prediction given in (12). Note that the
   time-variant period is given as $s(t + h) = \hat{r}_1(t|t)$.

Case #	Range of motion (mm)			Length	Evaluation coverage		Average period
	LR	SI	AP	T samples	t_s	t_e	$\bar{s}$
#1	0.7	10.2	1.5	3500 (116.7 s)	500 (16.7 s)	3500 (116.7 s)	91 (3.034 s)
#2	0.4	11.0	1.6	3228 (107.6 s)	501 (16.7 s)	3228 (107.6 s)	89 (2.968 s)
#3	0.5	10.9	1.6	3900 (130.0 s)	502 (16.7 s)	3900 (130.0 s)	91 (3.034 s)

Table 1. Brief summary of tested data sets. Range of motion is average distance from exhalation to
inspiration.

4. Time-variant SAR (TVSAR) model-based prediction given in (26).

Parameters for SAR and TVSAR models are summarized in Table 2.

4.1.3. Performance indexes

To evaluate the prediction performance, mean absolute error (MAE) was calculated. MAE is given as a function of prediction horizon h as follows.

$$\text{MAE}(h) = \frac{1}{t_e - t_s} \sum_{t=t_s}^{t_e} |e(t+h|t)| \tag{29}$$

Here t_s and t_e are lower and upper bounds for the evaluation shown in Table 1, and $e(t+h|t)$ is a prediction error defined by the Euclidean distance between the actual position and the predicted position.

The prediction error is calculated as follows.

$$e(t+h|t) = \sqrt{\sum_{i=1}^{3} (\hat{y}_i(t+h|t) - y_i(t+h))^2} \tag{30}$$

where $i = 1, 2$ and 3 denote LR, SI, and AP directions, respectively.

In addition to MAE, prediction success rate was adopted to evaluate the prediction efficiency for short treatment time. While treatment, the irradiation must be interrupted when unacceptable distance between the irradiated field and the target volume is detected for patient safety. Then, frequent prediction failure may prolong the treatment fraction. Thus, the rate of prediction success can discover better method. The prediction success rate (PSR) is defined as follows.

$$\text{PSR}(h) = \frac{\text{Number of successfully predicted samples}}{\text{Number of all evaluated samples}} \tag{31}$$

where the numerator is calculated as the number of the prediction errors within a threshold for tolerant accuracy. In this study, the threshold was set as 1 mm.

4.2. Results

Figure 16 shows 15 samples (0.5 s) forward prediction examples of tested methods. This examples were performed on SI direction of the data set #1. According to the prediction examples, SAR and TVSAR predictions seems smooth and similar to the actual position. Their errors are around zero, but sometimes the errors become larger than 2 mm. Also, there is a

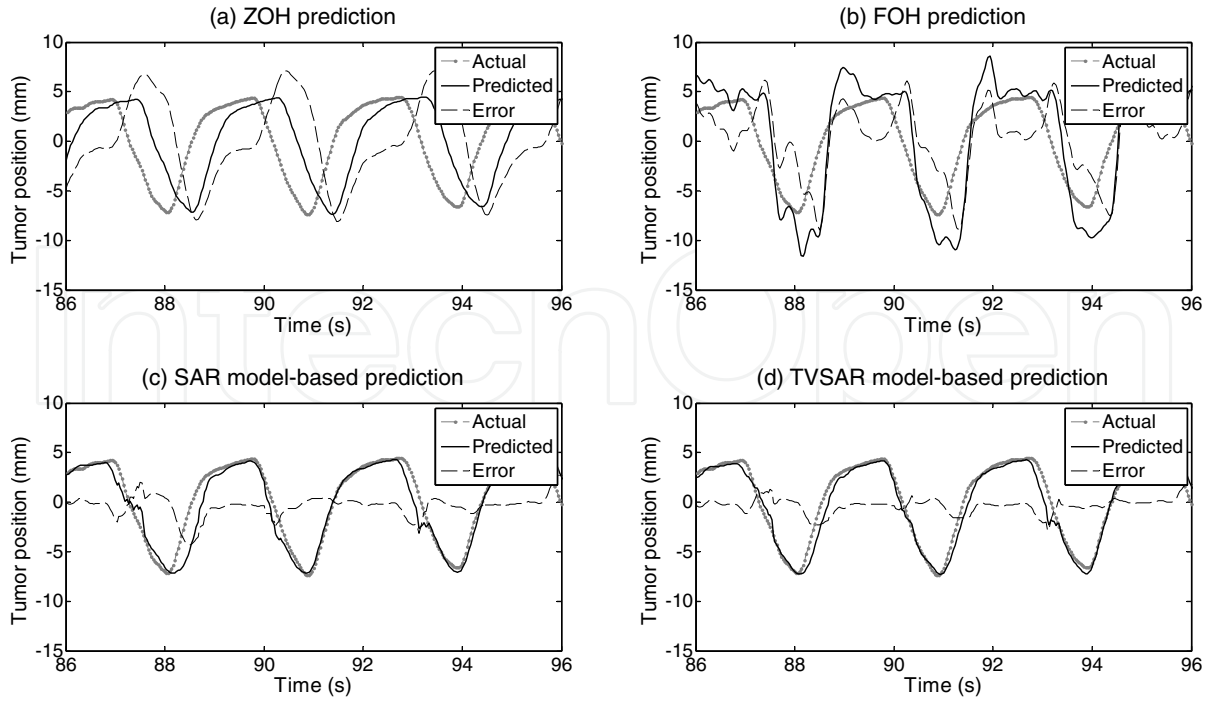| Parameters	
Order P	2
Coefficients $\Phi_\rho, \rho = 1, 2, \ldots, P$	$1/P$
Maximum lag for correlation function	400

Table 2. Parameters for SAR and TVSAR models

Figure 16. Examples of 0.5 s forward future prediction. (a) Zero-order hold, (b) First-order hold, (c)
Seasonal autoregressive model, and (d) Time-variant seasonal autoregressive model. Gray dots, black
lines, dashed lines denote actual position, predicted position, and distance between the actual and
predicted positions.

difference between SAR and TVSAR predictions at 87 to 89 s. Thus, TVSAR has provided
better prediction. On the other hand, ZOH and FOH predictions are noisy and not fitted into
the actual position. Their errors are frequently larger than 5 mm.

Figures 17 and 18 show MAE and PSR as a function of prediction horizon h/F_s (s). Each curves
of prediction performances drawn in the figures are averaged over the data sets. Also, error
bars indicates standard deviation of each performances for data sets variation.

As is clear from the figures, TVSAR is superior to SAR constantly. This suggests that the basic
concept of the TVSAR is more proper than SAR for the lung tumor motion prediction, i.e.,
reference intervals can work to improve the prediction accuracy for quasi-periodical nature.
Then, MAE and PSR curves of TVSAR are the least and the highest for prediction horizon
$h/F_s > 0.2$ s, respectively. It means that TVSAR is the first best method in the tested methods
for the radiotherapy machine with system latency of 0.2 s or longer. The average accuracy
and 70 % of the predicted samples respectively are sub-millimeter. This may suggest that
the TVSAR can perform tumor following irradiation during over 70 % of a single treatment
fraction.

SAR is the second-best, but the average error for prediction horizon longer than 0.5 s is over
1 mm. Note that the difference from TVSAR depends on the use of the second reference
interval in this experiment. Thus, unsuitable referring the past values by using the latest
period, $\rho \cdot s(t)$, increases the considerable prediction error.

ZOH and FOH are superior to SAR and TVSAR predictions for shorter prediction horizons
< 0.2 s. It is not remarkable because the position and velocity don't change drastically in
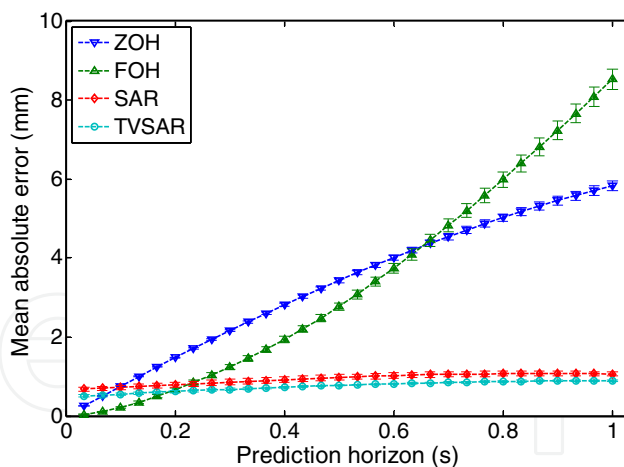short term in general. The periodicity in the respiratory motion quickly changes the position

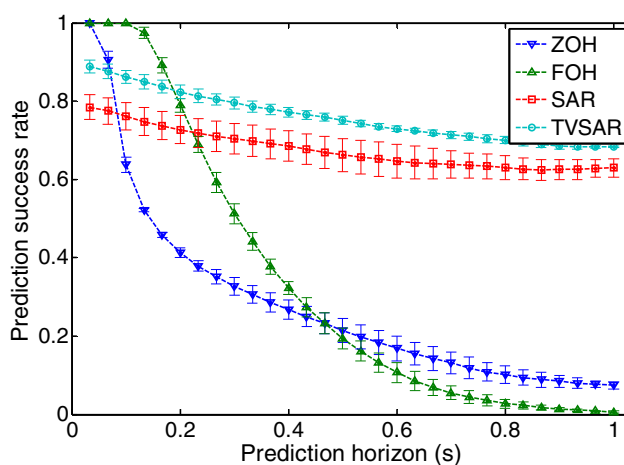**Figure 17.** Mean absolute error as a function of prediction horizon h/F_s (s).

Figure 18. Prediction success rate as a function of prediction horizon h/F_s (s).

and velocity at each peaks. Then ZOH and FOH cannot take into account the changes arisen. Therefore, their prediction errors drastically increase to unacceptable level with increase in prediction horizon. Those frequent and large prediction errors cause prolong the treatment fraction.

5. Conclusion

In this chapter, a prediction method of respiratory induced tumor motion for tumor following radiotherapy were introduced. The respiratory motion involves quasi-periodic nature as a dominant component and the motion causes unacceptable error of irradiation due to the system latency between tumor localization and beam-repositioning. To compensate the latency, prediction method of respiratory motion is very important and its prediction accuracy directly affects irradiation accuracy. Then, as a potent prediction method, time-variant seasonal autoregressive (TVSAR) model was introduced. TVSAR is an extended model of seasonal autoregressive model to be adaptable to the quasi-periodical nature. An experimental result by using clinical data sets of lung tumor motion showed the average accuracy of TVSAR is less than 1 mm for up to 1 s forward prediction and TVSAR is superior to other methods tested for <0.2 s ahead future prediction. Thus, TVSAR model-based prediction

method achieved accurate prediction of the respiratory tumor motion and can help the tumor
following irradiation.

Acknowledgements

Author details

Kei Ichiji
*Department of Electrical and Communication Engineering, Graduate School of Engineering, Tohoku
University, Sendai, Japan.*
Research fellow of Japan Society for the Promotion of Science (JSPS).

Noriyasu Homma and Makoto Yoshizawa
*Research division of Advanced Information Technology, Cyberscience center, Tohoku University,
Sendai, Japan.*

Masao Sakai
Center for Information Technology in Education, Tohoku University, Sendai, Japan.

Makoto Abe
*Department of Electrical and Communication Engineering, Graduate School of Engineering, Tohoku
University, Sendai, Japan.*

Norihiro Sugita
*Department of Management Science and Technology, Graduate School of Engineering, Tohoku
University, Sendai, Japan.*

6. References

[1] Onishi H, Araki T, Shirato H, Nagata Y, Hiraoka M, Gomi K, et al. Stereotactic
hypofractionated high-dose irradiation for stage I nonsmall cell lung carcinoma:
clinical outcomes in 245 subjects in a Japanese multiinstitutional study. Cancer.
2004;101(7):1623–1631.

[2] Shirato H, Suzuki K, Sharp G, Fujita K, Onimaru R, Fujino M, et al. Speed and
amplitude of lung tumor motion precisely detected in four-dimensional setup and
in real-time tumor-tracking radiotherapy. International journal of radiation oncology,
biology, physics. 2006;64(4):1229–1236.

[3] Suh Y, Dieterich S, Cho B, Keall P. An analysis of thoracic and abdominal tumour
motion for stereotactic body radiotherapy patients. Physics in medicine and biology.
2008;53(13):3623–3640.

[4] Keall P, Mageras G, Balter J, Emery R, Forster K, Jiang S, et al. The management of
respiratory motion in radiation oncology report of AAPM Task Group 76. Medical
physics. 2006;33(10):3874–3900.

[5] Purdy J. Current ICRU definitions of volumes: limitations and future directions. Seminars in radiation oncology. 2004;14(1):27–40.

[6] Kubo H, Hill B. Respiration gated radiotherapy treatment: a technical study. Physics in medicine and biology. 1996;41(1):83–91.

[7] Shirato H, Shimizu S, Kitamura K, Nishioka T, Kagei K, Hashimoto S, et al. Four-dimensional treatment planning and fluoroscopic real-time tumor tracking radiotherapy for moving tumor. International journal of radiation oncology, biology, physics. 2000;48(2):435–442.

[8] Keall P, Kini V, Vedam S, Mohan R. Motion adaptive x-ray therapy: a feasibility study. Physics in medicine and biology. 2001;46(1):1–10.

[9] Poulsen P, Cho B, Sawant A, Ruan D, Keall P. Detailed analysis of latencies in image-based dynamic MLC tracking. Medical physics. 2010;37(9):4998–5005.

[10] Poulsen P, Cho B, Ruan D, Sawant A, Keall P. Dynamic multileaf collimator tracking of respiratory target motion based on a single kilovoltage imager during arc radiotherapy. International journal of radiation oncology, biology, physics. 2010;77(2):600–607.

[11] Sharp G, Jiang S, Shimizu S, Shirato H. Prediction of respiratory tumour motion for real-time image-guided radiotherapy. Physics in medicine and biology. 2004;49(3):425–440.

[12] Ma L, Herrmann C, Schilling K. Modeling and prediction of lung tumor motion for robotic assisted radiotherapy. Intelligent Robots and Systems, 2007 IROS 2007 IEEE/RSJ International Conference on. 2007;p. 189–194.

[13] Bukovsky I, Ichiji K, Homma N, Yoshizawa M, Rodriguez R. Testing potentials of dynamic quadratic neural unit for prediction of lung motion during respiration for tracking radiation therapy. Neural Networks (IJCNN), The 2010 International Joint Conference on. 2010;p. 1–6.

[14] Mizuguchi A, Demachi K, Uesaka M. Establish of the prediction system of chest skin motion with SSA method. International Journal of Applied Electromagnetics and Mechanics. 2010;33(3):1529–1533.

[15] Ruan D. Kernel density estimation-based real-time prediction for respiratory motion. Physics in medicine and biology. 2010;55(5):1311–1326.

[16] Kalet A, Sandison G, Wu H, Schmitz R. A state-based probabilistic model for tumor respiratory motion prediction. Physics in medicine and biology. 2010;55(24):7615–7631.

[17] Verma PS, Wu H, Langer MP, Das IJ, Sandison G. Survey: Real-Time Tumor Motion Prediction for Image-Guided Radiation Treatment. Computing in Science & Engineering. 2011;13(5):24–35.

[18] Box G, Jenkins G, Reinsel G. Time series analysis. Holden-day San Francisco; 1976.

[19] Homma N, Sakai M, Endo H, Mitsuya M, Takai Y, Yoshizawa M. A new motion management method for lung tumor tracking radiation therapy. WSEAS TRANSACTIONS on SYSTEMS. 2009;8(4):471–480.

[20] McCall K, Jeraj R. Dual-component model of respiratory motion based on the periodic autoregressive moving average (periodic ARMA) method. Physics in medicine and biology. 2007;52(12):3455–3466.

[21] Ichiji K, Sakai M, Homma N, Takai Y, Yoshizawa M. SU HH BRB 10: Adaptive Seasonal Autoregressive Model Based Intrafractional Lung Tumor Motion Prediction for Continuously Irradiation. Medical Physics. 2010;37.

[22] Brockwell P, Davis R. Introduction to time series and forecasting. Springer Verlag; 2002.